# Simulation and Characterization of the Modulation Transfer Function in Fully Delineated Type-II Superlattices Infrared Detectors

D. Ramos, M. Delmas, R. Ivanov, L. Žurauskaitė, D. Evans, D. Rihtnesberg, L. Bendrot, S. Smuk, A. Smuk, S. Becanovic, S. Almqvist, P. Tinghag, S. Fattala, E. Costard, L. Höglund, and P. E. Hellström

***Abstract*— The modulation transfer function (MTF) in fully delineated 15 $\mu$m pitch type-II superlattice (T2SL) mid-wave infrared (IR) detectors is studied theoretically and experimentally. Theoretically, a 2-D model to simulate the spot scan (SS) profile is presented and used to compute the MTF as a function of the wavelength and the array geometry (pitch size, trench width). The dependence of the detector trench on the MTF is also evaluated experimentally by the edge spread function (ESF) method according to the ISO12233 standard. The experimental results show an excellent agreement with the theoretical model, reporting an MTF of 0.61 and 0.60 at the Nyquist frequency for 1 and 2 $\mu$m trench, respectively. With the simulation model, the effect of the increased optical crosstalk for smaller pixel pitch is discussed as a function of the trench width (0.5, 1, and 2 $\mu$m) and incidence angle up to $\pm$30°. Simulation results show MTF values at the Nyquist frequency between 0.61–0.62, 0.58–0.60, and 0.55–0.57 with an average degradation of 1%, 2%, and 7% at an angle of $\pm$30° compared to normal incidence for the 10, 7.5, and 5 $\mu$m pitch, respectively.**

***Index Terms*— Infrared (IR), modulation transfer function (MTF), optical crosstalk, type-II superlattices (T2SL).**

## I. Introduction

MID-WAVE infrared (3–5 $\mu$m, MWIR) imaging detectors benefit from the intrinsic uniformity and manufacturability of type-II superlattices (T2SL) [1]. Moreover, recent advancements in reducing the dark current density in these structures have enabled high operating temperatures while maintaining state-of-the-art performance allowing a significant reduction of the system's size, weight, and power [2]. Today, in the push for higher-resolution IR imaging detectors, the pixel pitch must be reduced below 15 $\mu$m [3], [4], which comes with several challenges.

The first one is related to the surface leakage current originating from the mesa sidewalls which can degrade the dark current density of small pixels [5]. The second is the loss of fill factor (in the case of delineated pixels), which can reduce the optical response of the array [6]. Finally, reducing the pixel pitch can lead to significant crosstalk effects [7], [8], [9], either electrically where the photo-generated carrier is collected by the neighboring pixel or optically where the photon is absorbed in the neighboring pixel. Increased interpixel crosstalk in small pitch formats compromises the resolution of the detector.

The metric to assess the resolution of a detector is the modulation transfer function (MTF), which describes how well the detector reproduces the contrast of the different spatial frequencies of the object. The MTF is the absolute value of the Fourier transform of the detector's point-spread function (PSF). Ideally, this corresponds to a square response given by the pitch size; however, the PSF can blur due to interpixel crosstalk. Therefore, for high-resolution formats, the MTF becomes a crucial indicator of the image quality and contrast in the arrays.

So far in the literature, only MTF measurements in MWIR T2SL detectors with pitch sizes larger than 20 $\mu$m have been reported [10], [11]. In addition, MTF simulation studies of T2SL detectors only employ planar or incompletely etched geometries [12], [13]. While these configurations aim to minimize surface leakage currents and maximize the fill factor by not exposing the mesa sidewalls with an interpixel trench, not fully delineating the pixel penalizes the MTF values mainly due to high electrical crosstalk [6], [12], [13]. However, state-of-the-art MWIR T2SL detectors implement a fully delineated geometry with appropriate passivation of the mesa sidewalls to suppress surface leakage currents [14], [15]. In addition, thanks to this geometry, optical concentration in

Manuscript received 2 November 2023; revised 5 January 2024; accepted 29 January 2024. Date of publication 14 February 2024; date of current version 26 March 2024. The review of this article was arranged by Editor L. Pancheri. *(Corresponding author: D. Ramos.)*

D. Ramos is with the KTH, 100 44 Stockholm, Sweden (e-mail: david.ramos@ir-nova.se).

M. Delmas, R. Ivanov, L. Žurauskaitė, D. Evans, D. Rihtnesberg, L. Bendrot, S. Smuk, A. Smuk, S. Becanovic, S. Almqvist, P. Tinghag, S. Fattala, E. Costard, and L. Höglund are with IRnova AB, SE-164 40 Stockholm, Sweden.

P. E. Hellström is with the KTH-Royal Institute of Technology, Electrum, School of ICT, SE-164 40 Kista, Sweden.

Color versions of one or more figures in this article are available at https://doi.org/10.1109/TED.2024.3361409.

Digital Object Identifier 10.1109/TED.2024.3361409

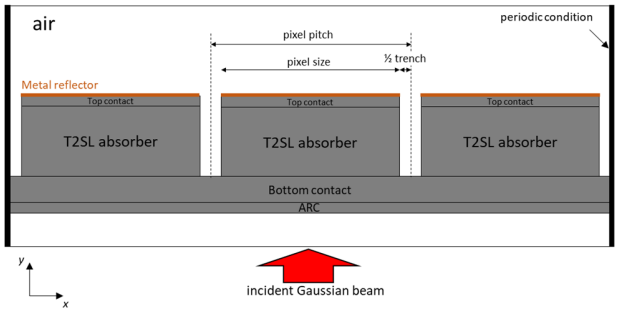


Fig. 1. COMSOL simulation geometry.

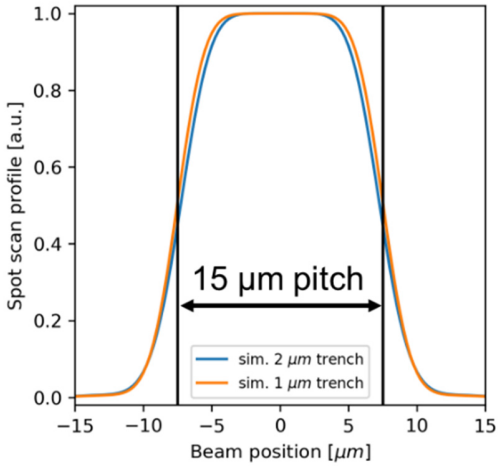


Fig. 2. Simulated SS profile for the absorption in the 3–5 $\mu$m spectral range for a fully delineated 15 $\mu$m pitch array with 1 $\mu$m and 2 trench.

the pixel has been observed as the pixel pitch reduces, thus mitigating the fill factor loss due to the trench etching and increasing the signal-to-noise ratio in smaller pixel size [7], [16], [17]. The pixels in such arrays are electrically isolated by etching a trench down in the semiconductor, consequently, only the optical crosstalk in the array geometry degrades the MTF.

In this context, this work reports the simulation and characterization of the MTF in fully delineated 15 $\mu$m pitch T2SL detectors. Initially, a 2-D model for calculating the spot scan (SS) profile is employed to compute the MTF dependency on trench width and wavelength. In the experimental section, the MTF of two 15 $\mu$m pitch 640 $\times$ 512 focal plane arrays (FPAs) with 1 and 2-$\mu$m trenches is determined using the slanted edge method described in ISO12233 standard with very good agreement with the simulation. Finally, the model is used to discuss the optical crosstalk in smaller pitch FPAs and the effect of the angle of incidence of the incoming light.

## II. Optical Simulation

Optical simulations were performed using the commercial software COMSOL Multiphysics[1]'s [18] and its wave optics module, which solves problems related to the propagation and interaction of electromagnetic waves in various optical systems.

A 2-D device geometry is used in the simulations, thus representing a cross section of the structure as illustrated in Fig. 1. Three adjacent pixels, with the detector stack presented in [2], are defined by trenches down to the bottom contact, as in the fabricated arrays. Since the pixels are fully reticulated along the absorber thickness (~4 $\mu$m), the electrical crosstalk can be neglected as all photogenerated carriers in the T2SL absorber of one pixel are collected by the same pixel. The Poisson's equation and continuity equations are therefore not solved, minimizing simulation runtimes. Periodic conditions are used at each side of the simulation domain mimicking an infinite linear array and boundary conditions are used to model the top metal as a perfect reflector. The meshing is performed with triangular elements with at least ten elements per wavelength (length depending on the local material properties) to resolve a wave properly [18].

A single-layer antireflective coating is also considered and as a first approximation, the air surrounds the linear array including within the trench, whilst experimentally a dielectric passivation layer is usually deposited on the pixel sidewall. As in 17, the T2SL material is modeled as a bulk material using the complex refractive index, $n + j\kappa$. The real part of the refractive index n is determined from the weighted average of the binary's bulk values, and the imaginary part $\kappa$ is determined from the measured absorption coefficient [19].

The simulation methodology employed in this work is similar to what has been reported in 20. In this case, rather than an ideal point source, the MTF is calculated for a Gaussian source, for which its contribution to the overall resolution is deconvolved in the Fourier space.

The incident electromagnetic field is defined by a Gaussian pulse propagating in the $y$-direction (normal to the array structure) and moving in the $x$-direction (from left to right in Fig. 1). The Gaussian pulse $\mathrm{gp}(x)$ is described by the following equation:

$$\mathrm{gp}(x) = \exp(-x^2/r^2) \tag{1}$$

with $r$ the beam radius. The Gaussian radius is chosen to be smaller than the pixel size so that the wavelength is maximum twice the Gaussian radius [20].

From this simulation, the integrated electromagnetic power loss, i.e., absorption, in the center pixel as a function of the Gaussian beam position defines the SS profile (alternatively to the PSF for an ideal point source). To be as close as possible to the experimental case for which a blackbody source is used, the SS is calculated for wavelength varying from 3 to 5 $\mu$m per 0.1 $\mu$m step. The total SS of the system is then the sum of all the SS profiles calculated at each wavelength. As an example, the total SS of a 15 $\mu$m pitch linear array with 1 and 2 $\mu$m trench is plotted in Fig. 2.

The MTF as a function of the spatial frequency $f_s$ can be calculated by performing the Fourier transform of the total SS which can then be deconvolved in the frequency domain with a component from the Gaussian source and another one from the detector by the following equation:

$$\mathrm{MTF}_t(f_s) = |\mathcal{F}\{\mathrm{SS}(x)\}| = \mathrm{MTF}_{\mathrm{GB}} \times \mathrm{MTF}_{\mathrm{det}}. \tag{2}$$

[1]Registered trademark.

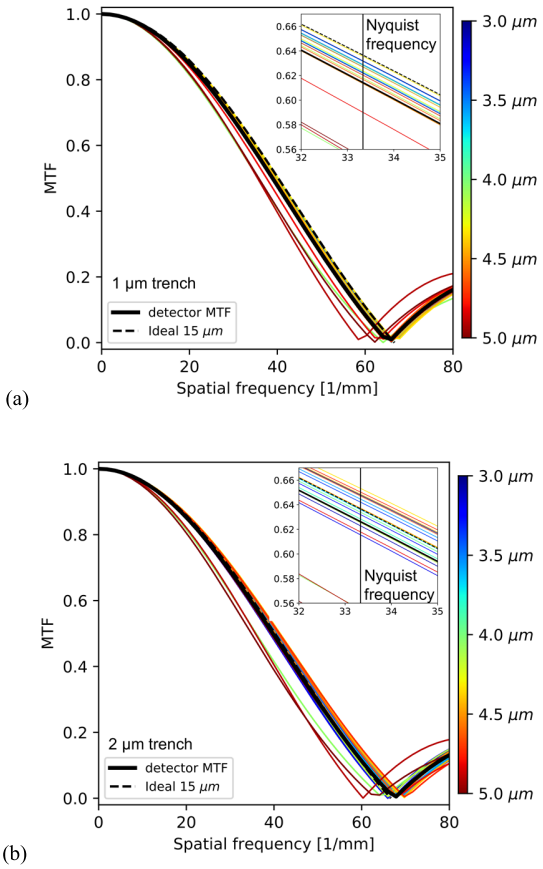


Fig. 3. Simulated MTF for the 3–5 $\mu$m spectral range of the fully delineated 15 $\mu$m pitch arrays with (a) 1 $\mu$m trench and (b) 2 $\mu$m trench. The inset shows a zoomed-in view around Nyquist frequency.

The Gaussian pulse MTF can be analytically calculated using the following equation:

$$\mathrm{MTF_{GB}} = \exp\left(\pi^2 f_s^2 r^2\right). \tag{3}$$

The MTFs reported in this section are the MTFs of the detector corrected by the contribution of the Gaussian beam and are usually compared with the ideal or footprint MTF which the sinus cardinal of $\pi f_s p$, with p the pixel pitch by the following equation:

$$\mathrm{MTF_{id}} = \sin\left(\pi f_s p\right)/\pi f_s p. \tag{4}$$

Fig. 3 shows the simulated MTF for a fully delineated 15 $\mu$m pitch array with 1 and 2 $\mu$m trench (from the corresponding SS profile plotted in Fig. 2) along with the ideal MTF. The MTF computed for all the incoming wavelengths is also displayed according to the color bar. The insets on the figure show a zoomed detail of the MTF curves around the Nyquist frequency, $f_{\mathrm{Nyq}} = 1/(2p)$.

For both cases, the low MTF curves, indicating high optical crosstalk, generally correspond to the longer wavelengths. This is attributed to the lower absorption coefficient at wavelengths close to the cut-off wavelength of the material. Only slight differences can be observed between the 1 and 2 $\mu$m trench arrays. The inset of the figures shows a higher spread of the MTF for a 2 $\mu$m trench. This suggests higher optical crosstalk associated with the broader trench and its higher impact on light propagation. However, the smaller pixel potentially increases the resolution capabilities of the detector array [11] which explains why for some wavelengths the MTF is higher than the ideal 15 $\mu$m pitch MTF; therefore, the impact of the higher crosstalk in this case is compensated by the smaller pixel size. The MTF at the $f_{\mathrm{Nyq}}$ is 0.61 and 0.62 for the 1 and 2 $\mu$m trench, respectively. These values are very close to the ideal value of 0.64 and far superior to the alternative planar structure simulated with T2SL materials [12], [13].

## III. MTF Measurements

Experimentally, the MTF is assessed using the slanted edge method, complying with the ISO 12 233 standard [21], [22]. This method is based on imaging a tilted edge onto the detector with respect to the array grating and projecting the data along the edge to obtain a super-sampled edge spread function (ESF). In this case, the MTF is calculated from the 1-D Fourier transform of the derivative of the ESF.

The main advantage of the slanted edge method lies in the extraction of the MTF by processing a single image, which simplifies the evaluation compared to other methodologies [10]. Additionally, when the edge is directly deposited onto the array, it eliminates the necessity for optical and vibration corrections, making it even more straightforward [21], [22]. This is a destructive method as it requires a sacrificial FPA; however, it is the approach adopted for this study.

Experimental results have established that data projection at the edge remains independent of the edge angle for angles below 10° [21], [22]. For a good ESF extraction and to avoid identical oversampling, the mask designed for this study incorporates edge angles of ±3.10°, ±4.50°, and ±5.85°.

The fabrication process of the MTF pattern starts with an already fabricated FPA. The mask is precisely aligned with the FPA using stepper lithography, achieving a misalignment of less than 0.006° across the entire FPA. Next, the metal layer is sputtered onto the sample and then removed in the open areas by lift-off process.

Fig. 4 illustrates the pattern deposited on the backside of the FPAs. Fig. 4(a) shows an image of the FPAs after fabrication, and Fig. 4(b) shows its signal response with ±10% contrast. Note that the pattern covers the entire FPA with multiple edges along both $x$- and $y$-directions, allowing the evaluation of the MTF uniformity across the FPA.

The patterned FPA's signal response is measured under 300 K blackbody illumination, with the pixel's signal being the integrated photocurrent from the overall response to radiation. Thus, the resolution information described by the MTF covers the cumulative effect of crosstalk across all detected wavelengths. Fig. 5(a) and (b) show the extracted MTF at different edges in both $x$- and $y$-direction of the 640 × 512/15 $\mu$m pitch MWIR T2SL FPAs with 1 and 2 $\mu$m trenches, respectively, along with the ideal MTF. The vertical dashed line on the figures indicates the Nyquist frequency.

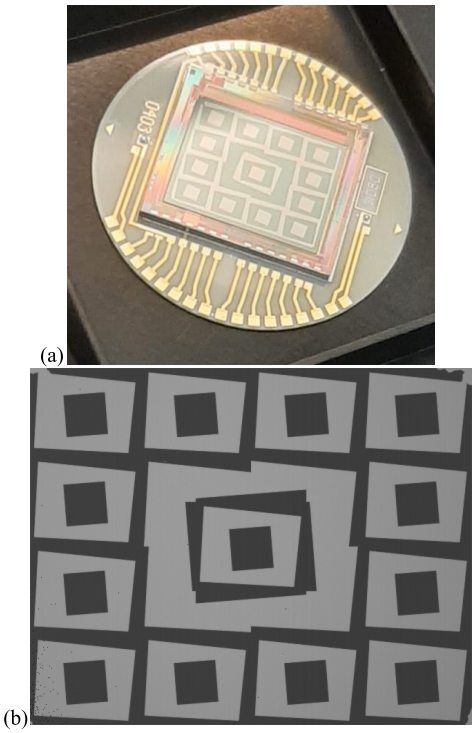


Fig. 4. (a) Image of the FPA after fabrication and (b) measured signal of a 640 × 512 15 $\mu$m pitch MWIR T2SL FPA with slanted edge pattern deposited on the backside.

Fig. 5 shows that there is no significant difference between multiple MTF curves extracted along the vertical and horizontal axis which is attributed to the uniformity and symmetry of the array grating. The average MTF with a 0.95 confidence interval at $f_{\mathrm{Nyq}} = 33.3\ \mathrm{mm}^{-1}$ is 0.60 $\pm$ 0.01 for the 1 $\mu$m trench and 0.61 $\pm$ 0.01 for the 2 $\mu$m trench. These values are very close to the ideal value of 0.64 and are also in excellent agreement with the simulation results. Moreover, these results complement the literature on fully delineated T2SL detector arrays in which values of 0.63 for the 30 $\mu$m pitch and 0.5 for the 24 $\mu$m pitch had been reported [10], [11].

The consistency between the simulations and the experimental data demonstrates the validity of the models and methods employed. It is worth noting that the experimental method calculates MTF over the total collected photocurrent, whereas the simulation focuses solely on the optical absorption. The complete delineation of the pixels makes the array's resolution unaffected by the collection efficiency of photogenerated carriers. Instead, it is the light-matter interaction that defines the detector's resolution in fully delineated T2SL FPAs.

## IV. Influence of Pixel Pitch, Trench Width, and Angle of Incidence on MTF

This section discusses the influence of the pixel pitch, trench width, and angle of incidence on the MTF using the same simulation methodology and the same detector structure as in Section II.

Fig. 6 shows the calculated MTF for a 10, 7.5, and 5 $\mu$m pitch array with a trench value of 0.5, 1, and 2 $\mu$m.

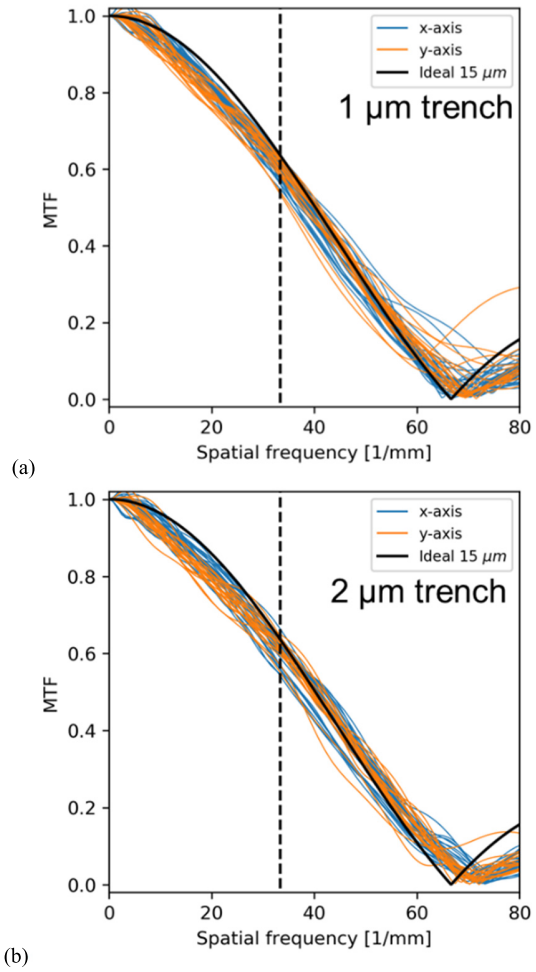


Fig. 5. MTF calculated from the measured ESF in $x$- and $y$-directions compared to the ideal MTF of a 15 $\mu$m pitch detector with (a) 1 $\mu$m trench. (b) 2 $\mu$m trench.

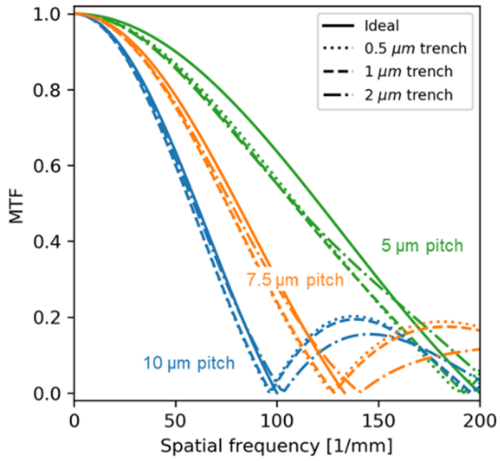


Fig. 6. Simulated MTF curves for the 3–5 $\mu$m spectral range of the fully delineated 10, 7.5, and 5 $\mu$m pitch arrays with 0.5, 1, and 2 $\mu$m trench.

The MTF curves correspond to the total SS computed for the incident radiation from 3 to 5 $\mu$m. The ideal values of the MTF corresponding to each pixel pitch are also included. The difference between the ideal MTF and the simulated

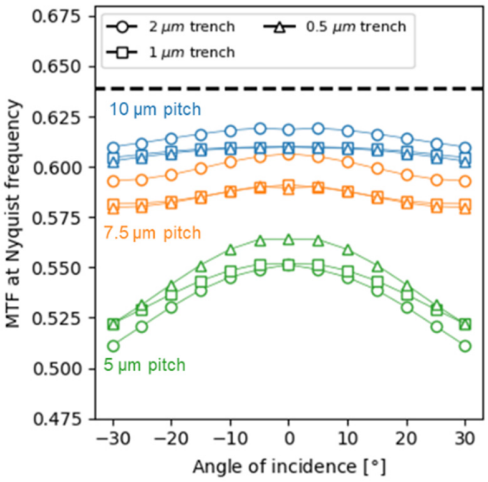


Fig. 7. MTF at the Nyquist frequency of the simulated MTF curves for the 3–5 $\mu$m spectral range of the fully delineated 10, 7.5, and 5 $\mu$m pitch arrays with 0.5, 1, and 2 $\mu$m trench as a function of the incidence angle.

MTF increases as the pitch decreases with MTF values at the Nyquist frequency between 0.61–0.62, 0.58–0.60, and 0.55–0.57 for the 10, 7.5, and 5 $\mu$m pitch respectively. This can be explained by an increased interpixel crosstalk due to the increased impact of the trench's diffraction on the pixels' absorption. Fig. 6 also shows the little spread of MTF curves with the trench. As in the 15 $\mu$m pitch, the higher crosstalk in the wider trench is compensated by higher resolution of the smaller pixel, therefore the trench width does not significantly impact the total MTF.

Despite the optical crosstalk, the delineation strategy remains superior to alternative planar detectors for which maximum MTF values at the Nyquist frequency of 0.55 have been reported for the 7.5 $\mu$m pitch [23]. However, unlike electrical crosstalk, the light-matter interactions that define optical crosstalk are anticipated to be dependent on the incidence angle of the light. This is especially important in small-pitch formats that often demand faster optics covering a broader range of incident angles [7], [24]. Therefore, this study is complemented by the simulation of dependance of the MTF on the incidence angle of the Gaussian pulse. Fig. 7 presents simulation results of the MTF at the Nyquist frequency as a function of the incidence angle for same pitch sizes (10, 7.5, and 5 $\mu$m) and trench dimensions (2, 1, and 0.5 $\mu$m).

Fig. 7 reveals a consistent trend: as the incidence angle increases, the MTF decreases, a behavior observed across all pitch and trench configurations. However, the higher optical crosstalk in the smaller pitch leads to a more significant degradation across the range of angles. For the 10 and 7.5 $\mu$m pitch, the degradation is minimal with average 1% and 2% reduction at an angle of 30° compared to normal incidence, however, for the 5 $\mu$m pitch, the MTF degrades by an average of 7%. These results highlight the importance of considering not only the MTF at normal incidence but also the potential detrimental effects of the incidence angle on optical crosstalk.

Nonetheless, the detector must be considered part of a larger system, especially for small pitches, such as the 5 $\mu$m. In this system, the field of view and photon flux, dictated by the optics, along with the characteristics of the read-out circuit and the detector, determines the system's resolution and sensitivity [24], [25]. For the resolution, the diffraction within the optical system often becomes the MTF limiting factor rather than the detector itself. The Airy diameter ($\emptyset = 2.44\,\lambda F$), governed by the wavelength and the $f$-number ($F$), defines the resolution limits. If $\emptyset$ is smaller or equal to the pitch size, the resolution is FPA-limited. Beyond this point, the optical system's influence on resolution becomes significant [24], [25]. Thus, the MTF of the detector is not the sole factor determining the imaging system's performance, as targeting the best sensitivity and resolution in an imaging system requires balancing multiple components.

## V. Conclusion

A 2D simulation model has been presented to compute the impact of optical crosstalk on the resolution of the detector. The MTF is simulated in the entire MWIR range and for 15 $\mu$m pitch arrays with 1 and 2 $\mu$m trenches. Correspondingly, the MTF is evaluated experimentally by post-processing two FPAs and using the ESF methodology. An excellent agreement between the experimental and calculated MTF of the arrays has been obtained for both 1 and 2 $\mu$m trenches with 0.60 and 0.61 values at the Nyquist frequency which is very close to the ideal resolution and sets the state-of-the-art for 15 $\mu$m pitch MW FPAs. The MTF simulations of 10, 7.5, and 5 $\mu$m pitch confirmed the increased optical crosstalk for reduced pixel pitch and increased incident angle. The presented model enables the evaluation of the device's geometry impact on the detector resolutions for pixel pitch compatible with Mpixel arrays.

## References

[1] D. Z-Y. Ting et al., "Type-II superlattice infrared detectors," in *Advances in Infrared Photodetectors*, vol. 84. USA: Elsevier Science & Technology, 2011, pp. 1–57, doi: 10.1016/B978-0-12-381337-4.00001-2.

[2] M. Delmas et al., "HOT MWIR T2SL detectors to reduce system size, weight, and power," in *Proc. 25th Sensors, Syst. Next-Gener. Satell.*, Sep. 2021, p. 118580Z, doi: 10.1117/12.2599856.

[3] R. G. Driggers, "Infrared detector size: How low should you go?" *Opt. Eng.*, vol. 51, no. 6, Jun. 2012, Art. no. 063202, doi: 10.1117/1.oe.51.6.063202.

[4] H. Lutz et al., "Towards ultra-small pixel pitch cooled MW and LW IR-modules," in *Proc. 44th Infr. Technol. Appl. XLIV*, May 2018, p. 106240B, doi: 10.1117/12.2304842.

[5] D. Ramos et al., "Quasi-3-dimensional simulations and experimental validation of surface leakage currents in high operating temperature type-II superlattice infrared detectors," *J. Appl. Phys.*, vol. 132, no. 20, p. 20, Nov. 2022, doi: 10.1063/5.0106878.

[6] O. Gravrand et al., "Discussion around IR material and structure issues to go toward small pixel pitch IR HOT FPAs," in *Proc. 46th Infr. Technol. Appl.*, Apr. 2020, p. 114070W, doi: 10.1117/12.2564572.

[7] A. Rogalski, "Scaling infrared detectors—Status and outlook," *Rep. Prog. Phys.*, vol. 85, no. 12, Dec. 2022, Art. no. 126501, doi: 10.1088/1361-6633/ac97a8.

[8] M. Vallone et al., "Quantum efficiency and crosstalk in subwavelength HgCdTe dual band infrared detectors," *IEEE J. Sel. Topics Quantum Electron.*, vol. 28, no. 2, pp. 1–9, Mar. 2022, doi: 10.1109/JSTQE.2021.3056056.

[9] B. Appleton, T. Hubbard, A. Glasmann, and E. Bellotti, "Parametric numerical study of the modulation transfer function in small-pitch InGaAs/InP infrared arrays with refractive microlenses," *Opt. Exp.*, vol. 26, no. 5, p. 5310, Mar. 2018, doi: 10.1364/oe.26.005310.

[10] J. Nghiem et al., "Study of the MTF of a MWIR T2SL focal plane array in IDDCA configuration," *Infr. Phys. Technol.*, vol. 96, pp. 192–198, Jan. 2019, doi: 10.1016/j.infrared.2018.11.004.

[11] S. B. Rafol et al., "Modulation transfer function measurements of type-II mid-wavelength and long-wavelength infrared superlattice focal plane arrays," *Infr. Phys. Technol.*, vol. 96, pp. 251–261, Jan. 2019, doi: 10.1016/j.infrared.2018.11.006.

[12] J. Schuster, "Assessment of the modulation transfer function in infrared detectors with anisotropic material properties: Type-II superlattices," *IEEE Trans. Electron Devices*, vol. 66, no. 3, pp. 1338–1344, Mar. 2019.

[13] J. Berthoz et al., "Range infrared detector issues in the SWAPc and pitch reduction context," in *Proc. Infr. Technol. Appl. XLVI*, May 2020, pp. 106–119, doi: 10.1117/12.2561306.

[14] M. Delmas et al., "Type-II superlattice detectors for high-performance SWaP detectors and HOT HD applications at IRnova," in *Proc. Infr. Technol. Appl. XLIX*, Jun. 2023, pp. 125340H–125340H9, doi: 10.1117/12.2663854.

[15] J. Jenkins et al., "Fabrication of small pitch, high definition (HD) 1k×2k/5$\mu$m MWIR focal-plane-arrays operating at high temperature (HOT)," in *Proc. 43rd Infr. Technol. Appl.*, Feb. 2017, p. 101771J, doi: 10.1117/12.2267879.

[16] P. Knowles et al., "Status of IR detectors for high operating temperature produced by MOVPE growth of MCT on GaAs substrates," in *SPIE Proc.*, Nov. 2012, Art. no. 854108.

[17] D. Ramos et al., "Optical concentration in fully delineated mid-wave infrared T2SL detectors arrays," *Appl. Phys. Lett.*, vol. 123, no. 18, p. 181102, Oct. 2023, doi: doi.org/10.1063/5.0176652.

[18] *Wave Optics Module:Analyze Micro- and Nano-Optical Devices*. Accessed: Feb. 1, 2023. [Online]. Available: https://www.comsol.com/wave-optics-module

[19] R. Ivanov et al., "T2SL development for space at IRnova: From eSWIR to VLWIR," in *Proc. 23rd Sensors, Syst., Next-Generation Satell.*, Oct. 2019, p. 1115111, doi: 10.1117/12.2533247.

[20] B. Pinkie and E. Bellotti, "Numerical simulation of spatial and spectral crosstalk in two-color MWIR/LWIR HgCdTe infrared detector arrays," *J. Electron. Mater.*, vol. 42, no. 11, pp. 3080–3089, Nov. 2013, doi: 10.1007/s11664-013-2647-3.

[21] F. Viallefont-Robinet et al., "Comparison of MTF measurements using edge method: Towards reference data set," *Opt. Exp.*, vol. 26, no. 26, p. 33625, Dec. 2018, doi: 10.1364/oe.26.033625.

[22] M. Estribeau and P. Magnan, "Fast MTF measurement of CMOS imagers using ISO 12333 slanted-edge methodology," in *Proc. Detectors Associated Signal Process.*, Feb. 2004, pp. 243–252, doi: 10.1117/12.513320.

[23] A. Yèche et al., "MTF characterization of small pixel pitch IR cooled photodiodes using EBIC," *J. Electron. Mater.*, vol. 49, no. 11, pp. 6900–6907, Nov. 2020, doi: 10.1007/s11664-020-08253-0.

[24] D. Lohrmann, R. Littleton, C. Reese, D. Murphy, and J. Vizgaitis, "Uncooled long-wave infrared small pixel focal plane array and system challenges," *Opt. Eng.*, vol. 52, no. 6, Jan. 2013, Art. no. 061305, doi: 10.1117/1.oe.52.6.061305.

[25] G. C. Holst and R. G. Driggers, "Small detectors in infrared system design," *Opt. Eng.*, vol. 51, no. 9, p. 096401, Sep. 2012, doi: 10.1117/1.oe.51.9.096401.